Electron/Atom Transfer in Halo-Bridged Homobimetallic Complexes. Structure and Donor−Acceptor Properties of Face-to-Face Dicopper Complexes with Teraazamacrocyclic Ligands

Manawadevi Y. Udugala-Ganehenege,[†] Mary Jane Heeg,[†] Lew M. Hryhorczuk,[†] Lowell E. Wenger,[‡] and John F. Endicott*[,†]

Department of Chemistry and Department of Physics, Wayne State University, Detroit, Michigan 48202

Received June 30, 2000

The syntheses and donor−acceptor properties of some novel, halo-bridged dicopper(II) complexes of α,α′-bis-(5,7-dimethyl-1,4,8,11-tetraazacyclotetradecane-6-yl)-*o*-xylene are reported. These complexes were characterized by their magnetic and electrochemical behavior, X-ray structure analysis, FAB mass spectroscopy, and electronic spectra. The bromo-bridged complex crystallized in the tetragonal system, space group *P*4(3)2(1)2, with a = 12.6584(5) Å, c = 28.6483 (14) Å, $Z = 4$, $R = 0.071$, and $R_w = 0.147$. The chloro-bridged complex crystallized in the monoclinic system, space group *C*2/*c*, with a = 32.749(2) Å, b = 18.8915(9) Å, c = 26.022(2) Å, β =114.831°, $Z = 12$, $R = 0.080$, and $R_w = 0.132$. Both molecules have C_2 symmetry. The two copper(II) ions are axially bridged by a bromine or a chlorine, and the two macrocycles are bridged by an *o*-xylene group. Each complex displays a cofacial ring arrangement. The Cu−X distance (where X = Cl, Br) is shorter than the sum of van der Waals radii of Cu and X. The phenyl ring is approximately orthogonal to the Cu−X−Cu axis. The nonhalo-bridged complex has a significant affinity for halides ($K_f \approx 10^4$ M^{-1}). The chloride-bridged complex had barely resolved differential pulse polarographic waves ($\Delta E_{1/2} \approx 28$ mV), while the bromide-bridged complex exhibited two CV waves in the 1.0−1.5 V range ($\Delta E_{1/2} = 0.24$ V). All the Cu^{II}/Cu^{I} couples were irreversible with a cathodic peak at about − 0.9 V. The magnetic susceptibility results below 20 K follow Curie−Weiss behavior, indicating that the magnetic interaction between the two Cu centers is weakly antiferromagnetic with $J \leq -1$ cm^{-1} for all three complexes. A bridging-ligand-mediated superexchange model is used to treat the magnetic and electron-transfer coupling in the $Cu^{II}(X^-)Cu^{II}$ complexes. A single set of perturbation theory parameters is consistent with the magnetic and electrochemical observations on the chloride-bridged complex and the magnetic properties of the bromide-bridged complex. The electrochemical behavior of the latter suggests a relatively low-energy, high-spin configuration for the $Cu^{III}(Br^-)Cu^{II}$ complex. The analysis attributes the weak Cu^{II}/Cu^{II} coupling to the orthogonality of the donor and acceptor orbitals to the bridging axis. It is inferred that bridging halide-mediated metal−metal dσ/pσ coupling significantly alters the chemical properties of the bimetallic complexes only when the donor and acceptor orbitals are coaxial with the bridging ligand. In such a limit, the coupling takes the form of a three-center bonding contribution.

Introduction

Long ago Orgel postulated[1] that electron-transfer rates should depend on the nature of the donor and acceptor electronic orbitals, and related concepts were shared in much of Taube's work at that time.[2] However, it has been extremely difficult to document such an "orbital dependence" of electron transfer rates largely because the rates of electron transfer tend to be dominated by nuclear reorganizational (or Franck−Condon, FC) contributions and no simple model systems have been available in which other tools can be systematically utilized. The "orbital dependence" of electron transfer should be most evident in inner-sphere electron transfer reactions because the transition-state geometry is relatively well defined for such processes. Furthermore, one expects, as argued in the early work, that among inner-sphere electron-transfer reactions the ones showing the largest effects will be those in which the donor and acceptor orbitals both have σ symmetry. However, a dependence of electron-transfer rates on purely electronic properties of the orbitals involved should appear as a contribution to the electronic matrix element, H_{DA}, and H_{DA} appears as a preexponential term in a typical treatment of electron-transfer rates, such as in the following:[3,4]

$$k_{nr} = \frac{4\pi^2}{h}(H_{DA}{}^2)(\mathrm{FC})$$

$$(\mathrm{FC}) = \sum_h \sum_j \frac{F_j\left[\exp\left(\frac{-(\Delta G_{DA}{}^\circ + jh\nu_h + \lambda_s)^2}{4\lambda_s k_B T}\right)\right]}{(4\pi\lambda_s k_B \mathrm{T})^{1/2}} \qquad (1)$$

$$F_j = \frac{S^j \exp(-S)}{j!}; \quad S = \frac{\lambda_h}{h\nu_h}$$

Equation 1 allows for contributions of both high-frequency, ν_h,

[†] Department of Chemistry.
[‡] Department of Physics.

(1) Orgel, L. E. In *Quelques Problemes de Chemie Minerale*; Report of the 10th Solvay Council; Université de Bruxelles: Bruxelles, Belgium, 1956; p 289.
(2) Taube, H. *Can. J. Chem.* **1959**, *37*, 129.
(3) Kestner, N.; Logan, J.; Jortner, J. *J. Phys. Chem.* **1974**, *64*, 2148.
(4) Gould, I. R.; Noukakis, D.; Luis, G.-J.; Young, R. H.; Goodman, J. L.; Farid, S. *Chem. Phys.* **1993**, *176*, 439.

10.1021/ic000726w CCC: $20.00
Published on Web 02/27/2001

and low-frequency (through λ_s) vibrational modes to the Franck−Condon factor; $h\nu_h \geq 4k_BT$ and $h\nu_s \leq 4k_BT$; $\Delta G_{DA}°$ is the free energy of reaction; and λ_i (i = h or s) is the reorganizational energy involving the modes indicated.

To our knowledge, there has been little direct experimental probing of the electronic coupling between dσ donor and dσ acceptor metal centers through a σ bond. Such coupling has long been presumed to be an element of inner-sphere electron-transfer reactions.[2,5] A kinetic comparison of the contrasts in reactivity for the $[Co(OH_2)_6]^{3+}$ and $[Co(OH_2)_5Cl]^{2+}$ oxidations of *trans*-M^{II}(MCL) complexes (MCL = a tetraazamacrocyclic ligand), based on a correction for differences in FC and using an argument based on the d orbital occupation in these complexes, has suggested that the effectiveness of a chloride-bridge-mediated pathway in electron transfer is strongly influenced by the spatial orientation of the donor orbital with respect to the bridging axis.[6] Thus, the bridged pathway was inferred to be ineffective for Cu^{II}(MCL) complexes because of the orthogonality of the copper-centered $d_{x^2-y^2}$ orbital (SOMO) to the bridging axis. In contrast, Margerum and co-workers[7] have postulated a favorable inner-sphere pathway for the rapid chloride-mediated electron-transfer rates of a Cu^{III}/Cu^{II} couple. The contrasting inferences illustrate some of the difficulties of kinetic approaches.

When the donor and acceptor are linked in a molecule, other more sensitive methods of investigating the factors that contribute to H_{DA} become available. Spectroscopic approaches have been extensively utilized.[4,8−14] The magnetic coupling between metals can also be used to investigate H_{DA}, but this approach has not been as much exploited, although Anderson's superexchange model for magnetic coupling, in which configurational mixing with electron-transfer excited states mediates the coupling,[15] has been adapted to a purely electron-transfer context as a superexchange model for bridge-mediated D/A coupling in electron-transfer systems.[16−18] The relationship between the magnetic and electron-transfer models of superexchange coupling has recently been reevaluated by Solomon and co-workers,[19,20] by Tuczek and co-workers,[21,22] and by Güdel and co-workers.[23,24] At least in the simple perturbation theory limit, the electronic coupling between paramagnetic ions and D/A electronic coupling in electron-transfer systems depend on very similar parameters with very similar functional relationships between those parameters (details are developed below). As a consequence of these similarities, magnetic coupling can be used as a reasonably sensitive probe of some aspects of electronic coupling in electron-transfer systems.

There are a vast number of studies of complexes with covalently linked transition metal donors (D) and acceptors (A).[9,10,19,25−27] These studies have most often involved covalently linked metals with dπ donor and dπ acceptor orbitals in which the bridging ligand has relatively low-energy π antibonding orbitals.[9,10] Studies of covalently linked dσ/dσ D/A systems have been rare. Yet, such systems were among the first well-characterized electron-transfer systems,[2,5] they are prototypes for the systematic study of "through bond" mechanisms of electron transfer, and they provide a clear mechanistic contrast to the typical dπ/dπ systems because "hole" transfer is expected to be the dominant pathway for electronic coupling in dσ/dσ systems and "electron" transfer is expected to be dominant in dπ/dπ systems when the bridging ligand has low energy antibonding π* orbitals. A problem in investigating dσ systems has been the design of simple molecules in which the transition metal donor and acceptor are in an appropriate geometry and in which the donor and acceptor orbitals can be relatively well defined with respect to the bridging moiety. An additional problem in synthesizing such systems is the very large ligand substitutional rate associated with partly or fully occupied dσ orbitals.[28] We have addressed these problems with tetraazamacrocyclic ligand complexes[29] and a synthetic approach based on the work of Kajiwara et al.[30,31]

This paper focuses on some dicopper−macrocyclic ligand complexes that assume a face-to-face geometry when a halide bridges the metals. Dicopper complexes are in principle capable of acting as two-electron acceptors or donors. The active sites of several metalloproteins contain one or more pairs of copper ions in proximity.[32−34] Cofacially arranged binuclear metalloporphyrins have been the subject of extensive investigation because these structural properties are thought to be relevant to catalytic activity.[32,33] The simpler cofacial macrocyclic ligand complexes allow a more critical spectroscopic evaluation of the behavior of the metals in such arrangements than do metalloporphyrin complexes because the intraligand optical absorptions are at relatively high energy and the spectroscopy is more sensitive to metal properties.

We have used magnetic, electrochemical, and spectroscopic properties of the cofacial macrocyclic ligand complexes to probe the halide-mediated Cu/Cu coupling in some simple halide-bridged dicoppper complexes. We have found that these

(5) Taube, H.; Myers, H.; Rich, R. L. *J. Am. Chem. Soc.* **1953**, *75*, 4118.
(6) Rotzinger, F. P.; Kumar, K.; Endicott, J. F. *Inorg. Chem.* **1982**, *21*, 4111.
(7) Anast, J. M.; Hamburg, A. W.; Margerum, D. W. *Inorg. Chem.* **1983**, *22*, 2139.
(8) Barbara, P. F.; Meyer, T. J.; Ratner, M. *J. Phys. Chem.* **1996**, *100*, 13148.
(9) Creutz, C. *Progr. Inorg. Chem.* **1983**, *30*, 1.
(10) Crutchley, R. *Adv. Inorg. Chem.* **1994**, *41*, 273.
(11) Graff, D.; Claude, J. P.; Meyer, T. J. In *Electron Transfer Reactions*; Isied, S. S., Ed.; ACS Advances in Chemistry Series 253; American Chemical Society: Washington, DC, 1997; p 183.
(12) Marcus, R. A. *J. Phys. Chem.* **1990**, *94*, 4963.
(13) Mulliken, R. S.; Person, W. B. *Molecular Complexes*; Wiley-Interscience: New York, 1967.
(14) Richardson, D. E.; Taube, H. *Coord. Chem. Rev.* **1984**, *60*, 107.
(15) Anderson, P. W. In *Magnetism*; Rado, G. T., Suhl, H., Eds.; Academic Press: New York, 1963; Vol. 1, Chapter 2.
(16) McConnell, H. M. *J. Chem. Phys.* **1961**, *35*, 508.
(17) Newton, M. D. *Chem. Rev.* **1991**, *91*, 767.
(18) Newton, M. D. *Adv. Chem. Phys.* **1999**, *106*, 303.
(19) Solomon, E. I.; Tuczek, F.; Root, D. E.; Brown, C. A. *Chem. Rev.* **1994**, *94*, 827.
(20) Brunold, T. C.; Gamelin, D. R.; Solomon, E. I. *J. Am. Chem. Soc.* **2000**, *122*, 8511.
(21) Vonseggern, I. V.; Tuczek, F.; Bensch, W. *Inorg. Chem.* **1995**, *34*, 5530.
(22) Tuczek, F.; Bensch, W. *Inorg, Chem.* **1995**, *34*, 1482.
(23) Schenker, R.; Weihe, H.; Gudel, H. U. *Inorg. Chem.* **1999**, *38*, 5593.
(24) Weihe, H.; Gudel, H. U.; Toftlund, H. *Inorg. Chem.* **2000**, *39*, 1351.
(25) Piotrowiak, P. *Chem. Soc. Rev.* **1999**, *28*, 143.
(26) Curry, W. B.; Grabe, M. D.; Kurnikov, I. V.; Skourtis, S. S.; Beratan, D. N.; Regan, J. J.; Aquino, A. J. A.; Beroza, P.; Onuchic, J. N. *J. Bioenerg. Biomembr.* **1995**, *27*, 285.
(27) Zamaraev, K. I.; Khairutdinov, R. F. *Top. Curr. Chem.* **1992**, *163*, 1.
(28) Wilkins, R. G. *Kinetics and Mechanisms of Reactions of Transition Metal Complexes*, 2nd ed.; VCH: Weinheim, Germany; 1991.
(29) Melson, G. A. *Coordination Chemistry of Macrocyclic Compounds*; Plenum: New York, 1979.
(30) Kajiwara, T.; Yamaguchi, T.; Oshio, H.; Ito, T. *Bull. Chem. Soc. Jpn.* **1994**, *67*, 2130.
(31) Kajiwara, T.; Yamaguchi, T.; Kido, H.; Kawabuta, S.; Kuroda, R.; Ito, T. *Inorg. Chem.* **1993**, *32*, 4990.
(32) Fillers, J. P.; Ravichandran, K. G.; Abdalmuhdi, I.; Tulinsky, A.; Chang, C. K. *J. Am. Chem. Soc.* **1986**, *108*, 417.
(33) Guilard, R.; Lopez, M. A.; Tabard, A.; Richard, P.; Lecomte, C.; Brandes, S.; Hutchison, J. E.; Collman, J. P. *J. Am. Chem. Soc.* **1992**, *114*, 9877.
(34) Collman, J. P.; Hutchison, J. E.; Wagenknecht, P. S.; Lewis, N. S.; Lopez, M. A.; Guilard, R. *J. Am. Chem. Soc.* **1990**, *112*, 8206.

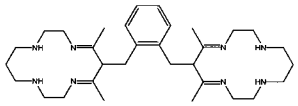

L

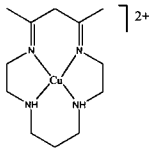

$[Cu([14]dieneN_4)]^{2+}$

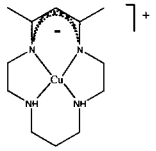

$[Cu([14]dienoN_4)]^{+}$

Figure 1. Skeletal structures of the ligands employed in this study.

complexes serve as unique models for examining the features of donor/acceptor (D/A) coupling in halide-bridged, inner-sphere electron (hole or "atom") transfer pathways.

Experimental Section

A. Preparation of Compounds. 5,7-Dimethyl-1,4,8,11-tetraazacyclotetradeca-4,7-dienato(−1)copper(II) Nitrate. [Cu([14]dieno(−1)N_4)]NO_3 and its protonated form, [Cu ([14]dieneN$_4$)]$(PF_6)_2$, were prepared according to the literature methods (see Figure 1for ligand structures and abbreviations[35]). The α,α′-dibromo-*o*-xylene was purchased from GFS chemicals and used without further purification.

***μ*-Bromo-α,α′-bis(5,7-dimethyl-1,4,8,11-tetraazacyclotetradeca-4,7-diene-6-yl)-*o*-oxylenedicopper(II) (LCu_2Br^{3+}) Complex (1).** Cu([14])dieno(−1)N_4)NO_3 (0.482 g, 1.38 mmol) was dissolved in absolute ethanol (25 mL). A slight excess of α,α′-dibromo-*o*-xylene (0.19 g, ∼0.69 mmol) was added to this green solution. The mixture was heated to reflux for 6 h, during which time the color of the solution turned from green to purple-red. The hot solution was filtered and the filtrate added dropwise to a saturated aqueous solution of NH_4PF_6. The resulting purple powder was isolated by filtration, washed with ether, and air-dried. Crystals suitable for X-ray structure determination were grown by dissolving the powder in hot 1 M NaBr aqueous solution and allowing it to come to room temperature slowly. Anal. Calcd for $Cu_2C_{32}H_{54}N_8BrP_3F_{18}$: C, 32.21; H, 4.57; N, 9.40;

Br, 6.80. Found: C, 32.34; H, 4.57; N, 9.22; Br, 7.06.

***μ*-Chloro-α,α′-bis(5,7-dimethyl-1,4,8,11)tetraazacyclotetradeca-4,7-diene-6-yl)-*o*-oxylenedicopper(II) (LCu_2Cl^{3+}) Complex (2).** The synthesis of this compound followed the procedure described for **1**. The filtered hot solution was added to a saturated aqueous $NaClO_4$ solution to obtain the final product. This appeared as a purple precipitate when the solution was cooled. The powder was separated and dissolved in hot 1 M NaCl aqueous solution and the solution cooled to room temperature to obtain very fine purple crystals. These fine crystals were dissolved in 1 M NaCl and left at room temperature for some time to obtain very dark irregular crystalline chunks that were suitable for X-ray structure determination.

Caution: The use of perchlorates in this preparation is potentially hazardous.

α,α′-Bis(5,7-dimethyl-1,4,8,11-tetraazacyclotetradeca-4,7-diene-6-yl)-*o*-oxylenedicopper(II) (LCu_2^{4+}) Complex (3). Removal of the bridging halide from **1** and **2** was accomplished by dissolving compound **1** or **2** (1 *μ*mol) in 10 mL of hot water and filtering the hot solution into a flask containing 1 M $AgNO_3$ (∼2 mL). The resulting mixture was filtered twice. The cherry-red filtrate was concentrated to a small volume and was added to a saturated, chilled (∼0° C) aqueous solution of NH_4PF_6. A pinkish-orange powder formed. This was isolated by filtering and dried on the frit of the funnel. Anal. Calcd for $Cu_2C_{32}H_{54}N_8P_4F_{24}$: C, 34.6; H, 4.9; N, 10.1; Found: C, 34.56; H, 4.87; N, 10.08.

Elemental analyses of C, H, N, and Br were performed by Midwest Micro Laboratory, Indianapolis, IN.

B. Instrumental Techniques and Physical Characterization. Visible and ultraviolet absorption spectra were determined in MeCN and H_2O using an OLIS modified Cary-14 spectrophotometer. Infrared spectra were determined in KBr pellets of the dry solids using a Nicolet 20DXM FT-IR spectrometer. FAB mass spectra were recorded on a Kratos MS 50 TC spectrometer with an NBA matrix. Cyclic voltamograms (CV) and differential pulse polarograms (DPP) were recorded in 0.1 M TBAH (tetrabutylammonium hexaflurophosphate) and 0.1 M TEAH (tetraethylammonium hexaflurophosphate) in MeCN using a BAS 100 electrochemical analyzer. The three-electrode assembly was comprised of the Pt working electrode, the Ag/AgCl reference electrode, and the Pt auxiliary electrode.

Magnetic susceptibility measurements were made using a Quantum Design model MPMS superconducting quantum interference device (SQUID) magnetometer, powder samples, a temperature range of 5−300 K, and a field strength of 10 000 Oe. Additional measurements were taken on pressed pellets of the powder. ESR spectra were recorded for a powder sample of complex **1** at room temperature using a Varian spectrometer operating in the X-band (9.5 GHz) with diphenylpicrylhydrazene (DPPH, $g = 2.0037$) as an external standard.

C. X-ray Structure Determinations. 1. Bromo-bridged Structure (1). Crystals were obtained as purple octahedra. A crystal $0.2 \times 0.2 \times 0.2$ mm^3 was mounted on Siemens/Bruker P4/CCD diffractometer equipped with monochromated Mo Kα radiation and the manufacturer's SMART collection software and SAINT processing software. A hemisphere of data were collected at 10 s/frame with 0.3° between each frame. A total of 31 150 reflections were integrated from the 1650 frames collected. Absorption corrections were applied with the program SADABS,[36] and 5541 reflections were obtained after averaging ($R_{int} = 0.062$). The structure was solved and refined on F^2 with the programs SHELXS and SHELXL-93.[35] Hydrogen atoms were placed in calculated or observed positions. All non-hydrogen atoms were anisotropically described. The asymmetric unit contains one-half of a bromo-bridged complex on a crystallographic 2-fold axis. The anions exhibit disorder in the fluorine arrangements, resulting in large thermal parameters for F atoms.

2. Chloride-Bridged Structure (2). Crystals were obtained as very dark irregular chunks. A large crystal $0.6 \times 0.4 \times 0.35$ mm^3 was mounted on the Siemens/Bruker P4/CCD diffractometer as described above. A hemisphere of data were collected at 10 s/frame with 0.3° between each frame. The 48 007 reflections were integrated from the 1650 frames collected. Absorption corrections were applied with the program SADABS,[36] and 17 228 reflections were obtained after averaging ($R_{int} = 0.072$). The structure was solved and refined on F^2 with the programs SHELXS and SHELXL-93.[36] Hydrogen atoms were placed in calculated positions. All non-hydrogen atoms were anisotropically described. The asymmetric unit contains 1.5 independent binuclear Cu complexes, 1.5 perchlorate anions, 3 Cl anions, and 10 solvent water molecules. The partial moieties are present on the 2-fold axis. In addition, there are other residual peaks on a ΔF map that may indicate partial occupancy by solvent, but these refine poorly when the additional solvent is included in the model. No hydrogen atoms were placed on the water solvent molecules. The loosely bound solvent is present in a network of hydrogen bonding along Cl^- anions in a vacant corridor between the layers of cations and perchlorates. There is a transformation available to describe the unit cell as hexagonal *R* with apparent space group $R\bar{3}c$ that requires $^1/_3$ of the *C*2/*c* asymmetric unit to be independent; however, the ligand and anions did not express this increased symmetry.

(35) Martin, J. G.; Cummings, S. C. *Inorg. Chem.* **1973**, *12*, 1477.

(36) Sheldrick, G. SHELXS-86, SHELXS-93, and SADABS; University of Göttingen: Göttengen, Germany, 1986, 1993, 1995.

Scheme 1. Synthesis of Bimetallic Copper Complexes

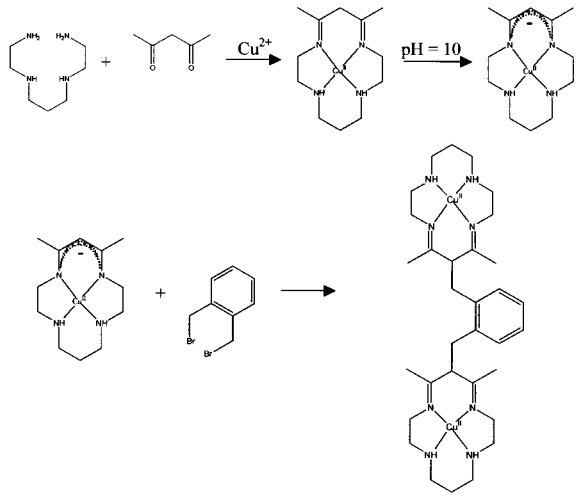

Table 1. Crystal Data and Structure Refinement

	$[LCu_2Br](PF_6)_3$	$[LCu_2Cl](ClO_4)_3 \cdot 6.66H_2O$
chemical formula	$C_{32}H_{53}BrCu_2F_{18}N_8P_3$	$C_{32}H_{67.33}Cl_4Cu_2N_8O_{10.67}$
fw	1192.73	1003.82
temp, K	295(2)	295(2)
wavelength, Å	0.710 73	0.710 73
space group	P4(3)2(1)2	*C*2/*c*
a, Å	12.6584(5)	32.749(2)
b, Å		18.8915(9)
c, Å	28.6483(14)	26.022(2)
β, deg	114.831(2)	
vol, Å^3	4590.5(3)	14510.9(14)
Z	4	12
density (calcd), mg/m3	1.726	1.369
abs coeff, mm^{-1}	2.011	1.149
final *R* indices [$I > 2\sigma(I)$]		
R1[a]	0.0711	0.0797
wR2[b]	0.1469	0.2469

[a] $R = \sum||F_o| - |F_c||/\sum|F_o|$. [b] $wR2 = [\sum w(F_o^2 - F_c^2)^2/\sum w|F_o^2)^2]^{1/2}$.

Results

A. Synthesis and Characterization. The binuclear Cu^{II} complexes have been prepared by the neucleophilic substitution reaction of $[Cu([14])dieno(-1)N_4)]NO_3$ with α,α′-dibromo-*o*-xylene in 2:1 molar ratio (Scheme 1). The product isolated from the preparative mixture was a bromide-bridged complex, **1**. This was first evident in the mass spectrum of the complex (Figure S19).[37] The X-ray and analytical data confirmed this analysis. That the dicopper complex sequesters one of the Br^- ions produced by nucleophilic displacement from dibromoxylene suggests a substantial affinity of the complex for Br^-. The bridging Br^- can easily be replaced by a Cl^- by recrystallizing complex **1** from 1 M NaCl. The bridging bromide or chloride can be removed with 1 M $AgNO_3$ to obtain the pink-orange nonhalo-bridged complex **3**. Complex **1** (or **2**) forms quantitatively on adding the appropriate halide to a solution of complex **3**. These observations confirm that the copper(II) complexes are axially labile, as expected.

B. Mass Spectroscopic Analysis. The FAB mass spectra of the bromo- and chloro-bridged complexes are shown in Figure S19.[37] These spectra were our first evidence that the complexes had sequestered halides, and they have been very useful in characterizing the molecules. The spectrum for the bromo-bridged complex shows three dominant ion peaks centered around $m/z = 1047$, 902, 757. These correspond to $\{[LCu_2Br](PF_6)_2\}^+$, $\{[LCu_2Br](PF_6) + e\}^+$, and $\{[LCu_2Br] + 2e\}^+$, respectively. The chloro-bridged complex has a molecular ion peak centered around $m/z = 911$ that is attributable to $\{[LCu_2Cl](ClO_4)_2\}^+$.

C. X-ray Structures. The molecular structures and the crystal packing motif are presented in Figures 3 and S20,[37] respectively. Crystallographic data for the structures of **2** and **1** can be found in Tables S1−S18[37] and are summarized in Table 1. The two macrocyclic rings (MCL) are arranged face-to-face, and the two copper(II) centers are axially bridged by a Br^- or Cl^-. The dihedral angles between mutual N_4 planes are 13.0° and 7.0° for the Br^-- and Cl^--bridged complexes, respectively. The bridging halide is equidistant from the two copper centers with angles of 165.6(6)° and 171.30(10)° for Cu−Br−Cu and Cu−Cl−Cu, respectively. The Cu−halide axes are nearly orthogonal to the N_4 planes of the macrocyclic ligands. The $[Cu(MCL)]_2X$ fragment of the complex has C_{2v} symmetry. The numbering scheme for the cations is shown in Figure 3, and the bond distances and angles are listed in Table 2. In both **1** and **2**, the N_4 equatorial coordination is planar (±0.001 Å for **1** and ±0.02 Å for **2**) and the copper atoms are displaced 0.26 Å out of the N_4 planes toward the axial halides. The Cu−Cu distance is 5.340 and 5.077 Å for **1** and **2**, respectively. The calculated distances of parallel atoms in two macrocycles (distance between macrocyclic rings), Cu−Cu distances, and dihedral angles are given in Table 3. The crystallographic data indicate the presence of two conformations for **2**, in contrast to the single conformation for **1**. A related dinickel complex has been shown to form an unsymmetrical, tetrameric chloro-bridged structure[31] and a symmetrical, dimeric bromo-bridged structure.[30]

D. Association Constants for Halide Binding in the $MCLCu^{2+}/Cu^{2+}MCL$ Cavity. Several attempts were made to obtain association constants for the equilibria represented in

$$[(L)Cu_2]^{4+} + X^- \rightleftarrows [(L)Cu_2X]^{3+} \quad (2)$$

and

$$[Cu([14]dieneN_4)]^{2+} + X^- \rightleftarrows \{Cu([14]dieneN_4)^{2+},X^-\}^+ \quad (3)$$

where $X^- = Cl^-$, Br^-, I^-, or NCS^-. Absorption bands of moderate intensity (10^3-10^4 M^{-1} cm^{-1}), assigned as ligand-to-metal charge-transfer (LMCT) bands, developed at wavelengths smaller than 400 nm as the halides associated with the copper complexes. The spectral changes that accompanied the successive addition of Br^-, I^-, and NCS^- to complex **3** are shown in Figure S21 of Supporting Information (the Cl^-/Cu^{II} LMCT bands of complex **2** occurred at wavelengths too deep in the UV to be easily deconvoluted from other absorptions).[37] A rapid increase in absorbance, due to the LMCT band, was observed even at small halide concentrations ($\leq 3 \times 10^{-3}$ M). Association constants for the halide (Br^-, I^-) association with complex **3** were estimated by comparing the maximum LMCT absorbance (at 281 nm for Br^- and at 358 nm for I^-) to the absorbance at various small halide concentrations. The formation constants in water were on the order of 10^4 M^{-1} (Table 4 and Figures S22 and S23[37]). The composition of acetonitrile solutions of the $[L(Cu)_2Br]^{3+}$ complex was investigated by observing visible and UV spectral changes after successive dilutions and in electrochemical studies of relatively concentrated solutions. Beer's law behavior was observed from ~4 ×

(37) Supporting Information; see paragraph at the end of this paper.

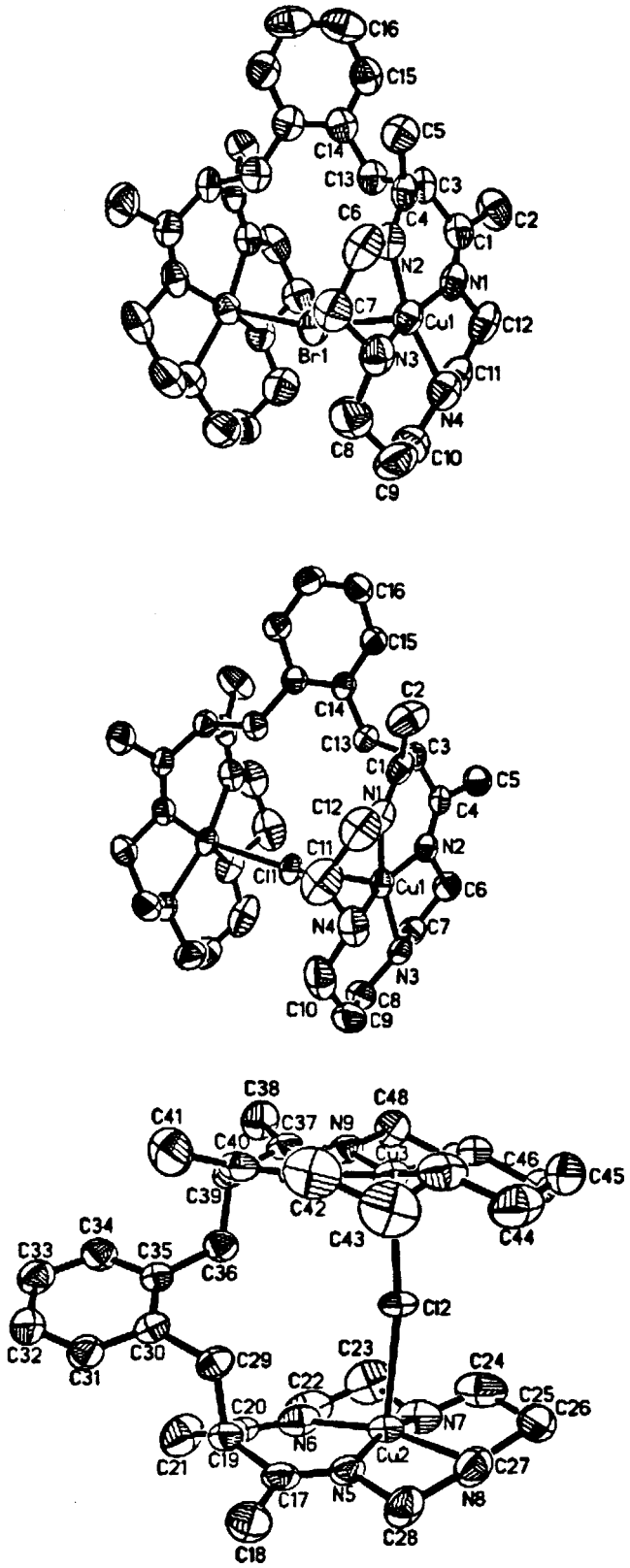

Figure 2. Molecular structures of the complexes: (top) $[L(Cu)_2Br]^{3+}$; (middle and bottom) isomers **1** and **2**, respectively, of $[L(Cu)_2Br]^{3+}$.

10^{-4} M to $\sim 10^{-5}$ M solutions. In this complex concentration range, there was an approximately 8% increase in absorbance and a 2 nm shift to higher energy of the d−d absorption band in a 0.1 M tetrabutylammonium hexafluorophosphate solution. Cyclic voltammograms and DPPs were obtained in acetonitrile solutions that varied from 7×10^{-3} to 5×10^{-4} M in the $[L(Cu)_2Br]^{3+}$ complex. The ratios of the current amplitudes of

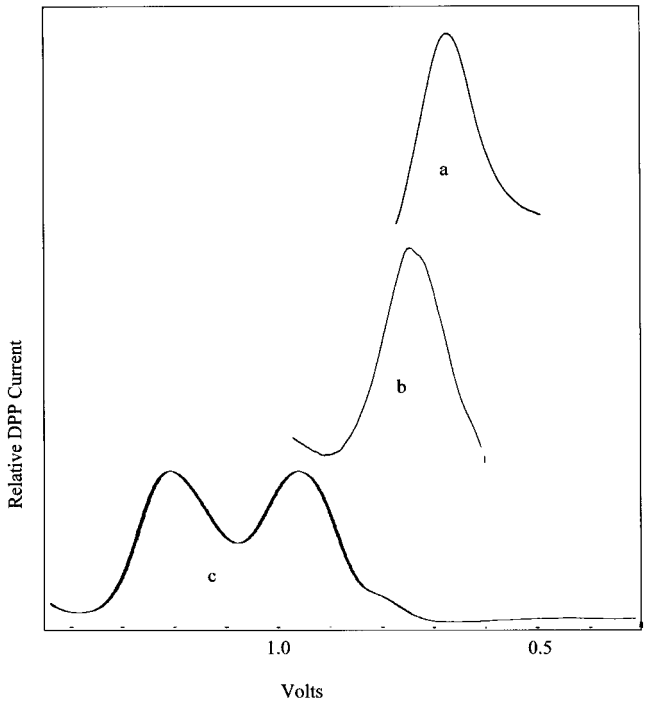

Figure 3. Differential pulse polarograms in acetonitrile: (a) $[Cu([14]\text{-dieneN}_4]^{2+}$; (b) $[L(Cu)_2Br]^{3+}$; (c) $[L(Cu)_2Br]^{3+}$. Units are volts vs Ag/AgCl.

the two peaks characteristic of this complex varied less than 15% over this concentration range; however, the current amplitudes (determined with respect to ferrocene in the same solution) decreased only about 8-fold over this concentration range. This effect suggests that the electroactive species was in equilibrium with a nonelectroactive species, such as a fine dispersion or precipitate.

Similar studies in water were complicated by the formation of precipitates. Association between the bimetallic complex and the halides reached equilibrium within our mixing times.

The I^- addition was done in the dark under aerobic as well as anaerobic conditions. On the basis of the LMCT absorption changes, the association constant for the I^- association of the monomer was found to be 27 ± 5 M^{-1} based on a plot of the inverse of the CT absorbance at ~350 nm vs concentration of I^-. These latter solutions decomposed after standing for several hours, forming I_3^- and a precipitate. The association of I^- with the $[LCu_2]^{4+}$ complex in acetonitrile results in the prompt formation of an absorption band at ~320 nm even with $[I^-] \leq 3 \times 10^{-3}$ M; however, this band disappears within a few minutes with the addition of excess I^-, or, more slowly, on leaving the sample at room temperature, and new bands form at ~287 and 360 nm. These are identical to the bands observed for I_2 in acetonitrile. This oxidation of I^- is accompanied by formation of a very fine precipitate.

E. Spectroscopy. The UV−visible spectra for the complexes are shown in Figure S24,[37] and the key spectroscopic parameters are given in Table 5. The bands in the UV region (below ~400 nm) are assigned as LMCT or intraligand electronic excitation. The nonhalide-bridged complex has a d−d transition at ~530 nm with $\epsilon \approx 165$ M^{-1} cm^{-1}. The bromo-bridged and chloro-bridged complexes exhibit one broad band in the visible region at 535 nm with the absorptivities $\epsilon = 333$ and 180 M^{-1} cm^{-1} per copper, respectively. The bandwidths of these d−d absorptions of the halide-bridged complexes (4.6×10^3 and 5.0×10^3 cm^{-1}, respectively) are 10−15% smaller than that of the $[L(Cu)_2]^{4+}$ complex. The higher intensity of the d−d band of

Table 2. Summary of Coordination Sphere Bond Lengths [Å] and Angles [deg]

(a) $[L(Cu)_2Br](PF_6)_3$ [a]

Cu(1)−N(1)	1.986(6)	N(2)−Cu(1)−Br(1)	97.8(2)
Cu(1)−N(2)	1.982(6)	N(3)−Cu(1)−Br(1)	96.7(2)
Cu(1)−N(3)	2.007(6)	N(4)−Cu(1)−Br(1)	96.8(2)
Cu(1)−N(4)	2.018(6)	Cu(1)−Br(1)−Cu(1)#1	165.64(6)
Cu(1)−Br(1)	2.6909(7)	C(7)−N(3)−Cu(1)	105.2(5)
N(1)−Cu(1)−N(4)	84.9(3)	C(8)−N(3)−Cu(1)	117.6(6)
N(2)−Cu(1)−N(3)	84.5(3)	C(11)−N(4)−Cu(1)	104.1(5)
N(2)−Cu(1)−N(4)	165.4(2)	C(10)−N(4)−Cu(1)	115.4(5)
N(3)−Cu(1)−N(4)	93.7(3)	C(1)−N(1)−Cu(1)	127.4(5)
N(1)−Cu(1)−N(2)	93.2(3)	C(12)−N(1)−Cu(1)	111.3(6)
N(1)−Cu(1)−N(3)	165.3(3)	C(4)−N(2)−Cu(1)	126.4(5)
N(1)−Cu(1)−Br(1)	98.0(2)	C(6)−N(2)−Cu(1)	111.6(5)

(b) $[LCu_2Cl](ClO_4)_3 \cdot 6.66H_2O$ [b]

(A) Molecule 1

Cu(1)−N(1)	1.968(5)	N(1)−Cu(1)−Cl(1)	96.70(14)
Cu(1)−N(2)	1.981(4)	N(2)−Cu(1)−Cl(1)	101.05(13)
Cu(1)−N(3)	2.010(4)	N(3)−Cu(1)−Cl(1)	97.61(13)
Cu(1)−N(4)	2.006(5)	N(4)−Cu(1)−Cl(1)	95.0(2)
Cu(1)−Cl(1)	2.5460(6)	Cu(1)#1−Cl(1)−Cu(1)	171.30(10)
N(1)−Cu(1)−N(2)	93.0(2)	C(7)−N(3)−Cu(1)	104.8(3)
N(1)−Cu(1)−N(3)	165.7(2)	C(8)−N(3)−Cu(1)	116.6(4)
N(2)−Cu(1)−N(3)	85.1(2)	C(10)−N(4)−Cu(1)	117.2(4)
N(1)−Cu(1)−N(4)	85.4(2)	C(11)−N(4)−Cu(1)	103.9(4)
N(2)−Cu(1)−N(4)	163.9(2)	C(7)−N(3)−Cu(1)	104.8(3)
N(3)−Cu(1)−N(4)	92.6(2)	C(8)−N(3)−Cu(1)	116.6(4)

(B) Molecule 2

Cu(2)−N(6)	1.971(5)	C(10)−N(4)−Cu(1)	117.2(4)
Cu(2)−N(5)	1.972(4)	C(11)−N(4)−Cu(1)	103.9(4)
Cu(2)−N(8)	2.003(5)	N(6)−Cu(2)−N(5)	92.6(2)
Cu(2)−N(7)	2.016(5)	N(6)−Cu(3)−N(8)	165.6(2)
Cu(2)−Cl(2)	2.5451(14)	N(5)−Cu(3)−N(8)	85.2(2)
Cl(2)−Cu(3)	2.5479(14)	N(6)−Cu(2)−N(7)	85.5(2)
Cu(3)−N(10)	1.963(5)	N(5)−Cu(2)−N(7)	163.6(2)
Cu(3)−N(9)	1.986(4)	N(8)−Cu(2)−N(7)	92.5(2)
Cu(3)−N(11)	2.001(5)	N(10)−Cu(3)−Cl(2)	96.80(14)
Cu(3)−N(12)	2.008(4)	N(9)−Cu(3)−Cl(2)	101.41(13)
N(5)−Cu(2)−N(7)	163.6(2)	N(11)−Cu(3)−Cl(2)	95.2(2)
N(6)−Cu(2)−Cl(2)	97.07(14)	N(12)−Cu(3)−Cl(2)	97.29(13)
N(5)−Cu(2)−Cl(2)	101.18(13)	C(17)−N(5)−Cu(2)	127.5(3)
N(8)−Cu(2)−Cl(2)	97.30(13)	C(28)−N(5)−Cu(2)	111.0(3)
N(7)−Cu(2)−Cl(2)	95.2(2)	C(20)−N(6)−Cu(2)	127.8(4)
Cu(2)−Cl(2)−Cu(3)	170.94(7)	C(22)−N(6)−Cu(2)	110.9(4)
N(10)−Cu(3)−N(9)	92.9(2)	C(24)−N(7)−Cu(2)	116.7(4)
N(10)−Cu(3)−N(11)	85.6(2)	C(23)−N(7)−Cu(2)	104.2(4)
N(9)−Cu(3)−N(11)	163.3(2)	C(27)−N(8)−Cu(2)	105.1(3)
N(10)−Cu(3)−N(12)	165.9(2)	C(26)−N(8)−Cu(2)	117.2(4)
C(40)−N(10)−Cu(3)	128.1(4)	C(37)−N(9)−Cu(3)	126.9(3)
C(42)−N(10)−Cu(3)	112.1(4)	C(48)−N(9)−Cu(3)	111.0(3)
C(44)−N(11)−Cu(3)	104.2(4)	C(40)−N(10)−Cu(3)	128.1(4)
C(47)−N12(39)−Cu(3)	105.6(4)	C(42)−N(10)−Cu(3)	112.1(4)
C(46)−N(12)−Cu(3)	117.0(4)	C(44)−N(11)−Cu(3)	116.6(4)
N(9)−Cu(3)−N(12)	84.9(2)	C(43)−N(11)−Cu(3)	104.2(4)
N(11)−Cu(3)−N(12)	92.6(2)	C(47)−N(12)−Cu(3)	105.6(3)
		C(46)−N(12)−Cu(3)	117.0(4)

[a] Symmetry transformations used to generate equivalent atoms: (#1) $y-1, x+1, -z$; (#2) $y, x, -z$. [b] Symmetry transformations used to generate equivalent atoms: (#1) $-x, y, -z+3/2$; (#2) $-x, y, -z+1/2$.

the bromo-bridged complex may be due to "intensity stealing" because the energy of the LMCT band is relatively low. The d−d absorption bands in all three bimetallic complexes are slightly red-shifted compared to the monomer, $[Cu([14]\text{-dieneN}_4)]^{2+}$ (Table 5). The small shifts in absorbance maxima and increases in absorptivity are characteristic of ion pair formation in this class of complexes.[38]

The initial spectrum of a mixture of $[L(Cu)_2]^{4+}$ and NaI in acetonitrile exhibits an absorption band with $h\nu_{max} = 30 \times 10^3$ cm^{-1} that we assign as an LMCT band. The $[L(Cu)_2Br]^{3+}$ complex has an intense band with $h\nu_{max} = 36.4 \times 10^3$ cm^{-1}, also assigned as LMCT. The energy difference of these bands is in good agreement with the energy difference (6.1×10^3 cm^{-1}) between the $\{Ru(NH_3)_6^{3+},I^-\}$ and $\{Ru(NH_3)_6^{3+},Br^-\}$ ion-pair charge-transfer (IPCT) absorption maxima.[39] The band observed in the $[L(Cu)_2Br]^{3+}$ complex is about 20 times more intense than the IPCT absorptions noted, but it is comparable to the absorptivity per Cu of the $\{Cu([14]\text{dieneN}_4)^{2+},I^-\}$ IPCT band. The distinction between IPCT and LMCT absorptions is probably not meaningful for axially associated ligands in these $Cu(MCL)^{2+}$ systems. That the absorptivity per Cu is comparable for the "ion pair" and $[L(Cu)_2Br]^{3+}$, and the single higher energy CT absorption of the latter, suggests that the two copper centers are not appreciably mixed in the LMCT Franck−Condon excited state. We have not resolved, or attempted to assign, the higher energy absorptions of these complexes.

Oxidations of the complexes with $Ce(aq)^{4+}$ or $Co(OH_2)_6^{3+}$ did not generate detectable transient absorptions in the 30 s to 1 min mixing times. The absorptions characteristic of the macrocyclic ligand complexes of Cu(II) did bleach in these experiments, and the "baseline" absorption increased throughout the visible−UV spectral region in a manner typical of the formation of a heterogeneous dispersion.

The IR spectrum for the bromo-bridged complex is shown in Figure S25.[37] The sharp peak at 3267 cm^{-1} and a single strong

Table 3. Intramolecular Contact Distances[a] (Å) and Dihedral[b] Angles (deg) between Related Atoms of the Macrocyclic Rings in the Halo-Bridged Dicopper Complexes

	$[LCu_2Br](PF_6)_3$	$[LCu_2Cl](ClO_4)_3 \cdot 6.66H_2O$
Cu(1)···Cu(1)	5.340	5.077
C(8)···C(10)	5.548	4.896
C(10)···C(8)	5.547	
C(10)···C(10)	5.260	6.027
C(8)···C(8)	6.598	4.672
C(9)···C(9)	6.650	5.791
C(9)···C(8)		5.058
C(2)··· C(3)		5.077
C(24)···C(46)		4.874
C(25)···C(46)		5.018
C(26)···C(46)		4.640
C(26)···C(45)		5.036
C(26)···C(44)		4.84
dihedral angle[b]	13.0	6.8 and 6.7

[a] esd's ≤ 0.1 Å. [b] Between the N_4 planes of the macrocyclic rings.

Table 4. Approximate Molar Equilibrium Constants (K) for the Association of $[L(Cu)_2]^{4+}$ and the Monomer with Various Anions at 25 °C

anion	complex	solvent	K,[a] M^{-1}
I^-	$[Cu([14]\text{dieneN}_4)]^{2+}$	MeCN	27 ± 5
Br^-	$[L(Cu)_2]^{4+}$	H_2O	$(2 \pm 1) \times 10^3$ [b]
Br^-	$[L(Cu)_2]^{4+}$	MeCN	$\geq 5 \times 10^3$
Cl^-	$[L(Cu)_2]^{4+}$	MeCN	$>10^2$ [c]

[a] Based on the LMCT absorption band except as noted. [b] pH = 4. See Figure S4. [c] Based on changes in ligand field absorbance at ~500 nm.

Table 5. Absorption Spectra of the Complexes in Acetonitrile

complex	λ_{max}, nm (ϵ/Cu, M^{-1} cm^{-1}) [$\Delta\nu_{1/2}$, cm^{-1}]
$[Cu([14]\text{dieneN}_4)]^{2+}$	497 (132) [5700]; 266 (~600)
$[L(Cu)_2Br]^{3+}$	536 (313) [4600]; 282 (2740)
$[L(Cu)_2Cl]^{3+}$	535 (180) [5000]; 270 (1100)
$[L(Cu)_2]^{4+}$	529 (165) [5500]; 250 (990)
$\{[L(Cu)_2]^{4+} + I^-\}$	320 ($\geq 2 \times 10^3$)

(38) Palmer, J. M., Papaconstantinou, E.; Endicott, J. F. *Inorg. Chem.* **1969**, *8*, 1516.

(39) Waysbort, D.; Evenor, M.; Navon, G. *Inorg. Chem.* **1975**, *14*, 514.

Table 6. Estimated Magnetic Parameters Using $1/\chi_M$ vs Temperature Plots for $T < 20$ K

complex	slope, (mol Oe)/(emu K)	*C*, (emu K)/(mol Oe)	Θ, K	*J*, cm^{-1}
$[L(Cu)_2][PF_6]_4$	1. 7768	0.573	−0.53	−1.47
$[L(Cu)_2Cl][ClO_4]_3$	1.307	0.765	−0.17	−0.47
$[L(Cu)_2Br][PF_6]_3$	1.7443	0.563	−0.21	−0.58

peak at 1675 cm^{-1} are similar to absorptions of the monomer, and they are assigned as NH and C═N stretching modes, respectively.

F. Electrochemistry. The complexes have been characterized by cyclic voltammetry (CV) and differential pulse polarography (DPP) in the potential range 500−1800 mV and with different scan rates (Table 6). For $[L(Cu)_2Br]^{3+}$ we observed two CV waves in the 800−1500 mV range (Table 6; Figure S26[37]). A single CV wave was observed for $[L(Cu)_2Cl]^{3+}$ at ∼700 mV (vs Ag/AgCl; Figure S26[37]). The DPP scans of these complexes and $[Cu([14]dieneN_4)]^{2+}$ are shown in Figure 3. Two peaks separated by 0.26 V were resolved in DPP scans for the bromo-bridged complex, but DPP scans suggested about a 25 mV separation of peaks for the chloro-bridged complex (Figure 3). No peak separation was observed for $[Cu([14]dieneN_4)]^{2+}$. The CVs of $[L(Cu)_2]^{4+}$ were irreversible with an anodic peak at about 0.8 V and a cathodic peak (or peaks, depending on the scan range and rate) near 0.4 V. This contrast in behavior with the $[Cu([14]dieneN_4]^{2+}$ monomer suggests a relatively facile two-electron oxidation of the ligand in the dimer (the deprotonated form of [14]dieneN$_4$ ligand, p$K_a \approx 6$, is very easily oxidized;[40] a qualitatively similar two-electron oxidation of a related *β*-diimine−macrocyclic ligand coordinated to cobalt(III) has been previously observed[41]). That similar irreversibility is not found for the halo-bridged dicopper complexes suggests some electrostatic stabilization of those complexes.

Irreversible reductions of the $[L(Cu)_2X]^{3+}$ complexes occurred between −0.5 and −1.3 V. At the most negative potentials, these electrochemical reductions were complicated by the formation of CuX and/or (depending on the sweep rate and range) Cu^0. A poorly formed wave with $E_{pc} = -0.9$ is apparently characteristic of all the macrocyclic complexes in this study and is attributed to the Cu^{II}/Cu^{I} couple.

G. Magnetic Properties. To determine the magnetic interaction between the two copper centers in each of the complexes, the temperature dependence of the magnetic susceptibility χ_M was measured in the 5−300 K range. Only at temperatures below 20 K did the data exhibit a Curie−Weiss behavior ($\chi_M = C/[T - \Theta]$) as shown by the linear behavior of the inverse magnetic susceptibility as a function of temperature in Figure S27.[37] The paramagnetic Curie temperature Θ for all three data sets is slightly less than 0 K and indicative of very weak antiferromagnetic interactions between the Cu^{II} centers for all three complexes. Assuming a dimer model with an exchange interaction *J* between the Cu^{II} centers of spin $S = {}^1/_2$, the data results in $J \cong -0.58$, −0.47, and −1.47 cm^{-1} for the bromo-bridged, chloro-bridged, and nonhalo-bridged complexes, respectively (Table 6). While the Curie constant *C* for the chloro-bridged complex is approximately equal to the expected value of 0.750 emu K mol^{-1} Oe for Cu dimers with $S_1 = S_2 = {}^1/_2$, the Curie constants for the bromo-bridged and nonhalo-bridged complexes are approximately 25% less. This is evident in a plot of the effective magnetic moment μ_{eff} vs temperature (Figure S28[37]). The effective magnetic moment is determined using

$$\mu_{eff} = \left[\frac{3k_B}{2N_A(\mu_B)^2}\right]^{1/2}\left[\frac{d(\chi^{-1})}{dT}\right]^{-1/2} \quad (4a)$$

or

$$\mu_{eff} = 2\left[\frac{d(\chi^{-1})}{dT}\right]^{-1/2} \quad (4b)$$

where χ_M is in units of emu/Oe per mole of compound (i.e., per pair of Cu^{II} ions), μ_B is the Bohr magneton, N_A is Avogadro's number, and k_B is Boltzmann's constant. The magnetic moments (per copper) for both the bromo-bridged and nonhalo-bridged complexes are approximately 1.51 μ_B from the susceptibility results, while that for the chloro-bridged complex is 1.75 μ_B These differences could possibly arise from the difference in molecular orientation in the unit cells of the PF_6^- and ClO_4^- salts (see Figure S20[37]) or they might arise from a substantial (∼25%) Cu(I) impurity. Elemental analyses, mass spectroscopic data, visible spectroscopy, and general chemical behavior are not consistent with such a significant Cu(I) impurity, but the compounds do not appear to be stable for extended periods of time, even in the solid state, and the possibility of some impurity cannot be entirely excluded.

The ESR spectra for the powder samples of $[L(Cu)_2Br]^{3+}$ and of $[Cu([14]dieneN_4)]^{2+}$ at room temperature obtained in the X-band region were nearly isotropic. The resonances were centered at 3.27 kG with average *g* values of 2.071 with respect to the DPPH marker. This gives rise to μ_{eff} of 1.79 μ_B This is a more direct measurement of the molecular magnetic moment than is the bulk susceptibility.

Discussion

In this study we have synthesized and characterized some simple face-to-face dimeric copper(II) complexes. We have used these complexes to evaluate the hypothesis that orbital orientation, and the resulting overlap with a bridging ligand, can significantly affect the electron-transfer properties of a reactant system. We have direct comparisons of electronic coupling in the electron-transfer systems to that inferred from the magnetic studies.

A. Structural Properties of the Complexes. 1. Molecular Structure. In the course of this work we have found that linking two copper−macrocyclic ligand complexes by *o*-xylene results in some novel chemical properties. The tetraaza-macrocyclic rings of these complexes constrain the electronic distribution so that the partly filled dσ orbital of Cu(II) lies in the plane of the four nitrogen donors (this is commonly named a "$d_{x^2-y^2}$" orbital, but the local Cu-centered axis labels are not appropriate to these molecules; we will designate this orbital as d$\sigma_{||}$), and this spatial region is shielded from interaction with other potential donors by the atoms of the macrocyclic ring. Thus, the closest interactions with donors are constrained to be axial and nearly orthogonal to the N_4 planes.[29,38] Axial interactions with halides will maximize Coulombic attractions. These points are illustrated in the solid-state structures of the $[L(Cu)_2X]^{3+}$ complexes. The *o*-xylene linkage is flexible, and a molecular mechanics examination of a simplified, neutral model of the ligand moiety indicates that there is little difference in energy for different rotational arrangements of the MCL moieties. In solution, and in the absence of anions of the appropriate size, the lowest energy conformations would place the two cationic copper centers far away from each another. Very weak electronic

(40) Switzer, J. A.; Endicott, J. F.; Khalifa, M. A.; Rotzinger, F. P.; Kumar, K. *J. Am. Chem. Soc.* **1983**, *105*, 56.
(41) Watzky, M. A. Ph.D. Dissertation, Wayne State University, Detroit, MI, 1994.

mixing along the bridging axis could account for the very weak magnetic coupling found in the complexes.

2. Dicopper Complex Chelation of Halide Ions. The simple dicopper complexes reported here have high affinities for the complexation of halides, with the dicopper complex acting as a "chelating" ligand for the halide. For example, the ratios of formation constants of Mg^{2+} and Ca^{2+} complexes with oxalate to those with acetate are 150 and 59, respectively.[42] The ratio of the formation constant for the $[L(Cu)_2Br]^{3+}$ complex to that for the $\{[Cu([14]dieneN_4)]^{2+},I^-\}$ ion pair is about 50 in water. The binding of the halide to the $[L(Cu)_2]^{4+}$ complex is probably largely ionic, as in the ion pair. This is consistent with expectation based on doubly occupied axial orbitals (HOMO's) of each Cu(II). There is no simple basis for a significant covalent bonding interaction across the halide bridge between the macrocyclic copper complexes.

B. Magnetic Coupling. 1. Electronic Coupling in the Electron-Transfer Systems. The relatively simple UV−visible spectroscopy (only one LMCT band and no detected metal-to-metal charge-transfer band) and the electrochemical behavior of $[L(Cu)_2Cl]^{3+}$ are experimental manifestations of relatively weak electronic coupling. However, there appears to be some contradiction between the weak electronic coupling implied by the magnetic and spectroscopic behavior of $[L(Cu)_2Br]^{3+}$ and its electrochemical properties. These and other features of the D/A electronic coupling in the chloride- and bromide-bridged copper complexes provide insight into D/A coupling in transition metal systems.

2. Magnetic Coupling in These and Related Systems. The magnetic properties of the halide-bridged complexes indicate that there is little detectable halide-mediated coupling of the copper(II) centers in the face-to-face bis-macrocyclic complexes. This is consistent with the orthogonality to the bridging axis of the partly filled $d\sigma_{||}$ SOMOs at each copper(II) center. This contrasts with the significant antiferromagnetic coupling found in bridged bis-Cu^{II}(MCL) complexes in which the copper coordination geometry is appreciably distorted toward a trigonal-bipyramidal geometry: $J = -4.8$ cm^{-1} for μ-cyano-bis(5,7,7,-12,14,14-hexamethyl-1,4,8,11-tetraazacyclotetradeca-4,1-diene)-dicopper(II) perchlorate;[43] $J = -144$ cm^{-1} in μ-chloro-bis(5,7,7,12,14,14-hexamethyl-1,4,8,11-tetraazacyclotetra-decane)dicopper(II) perchlorate ($[\{Cu(tet\textit{b})\}_2Cl]^{3+}$).[45] The N−Cu−N angles in the approximate trigonal planes of these complexes (the bridging CN^- or Cl^- forms the remaining trigonal vertex) are 134° and 115°, respectively. In the systems reported here the comparable angles are approximately 165°. Thus, the magnetic moment in these complexes increases in magnitude as the local Cu(II) environment of the bimetallic complexes changes from square pyramidal to trigonal bipyramidal. The earlier proposal[43] that the variations in magnetic coupling arose largely from variations in the Cu−Cu distance is inconsistent with our observations. It seems more likely that the variations in magnetic coupling among these closely related tetraaza-macrocyclic liganded copper(II) complexes arise from differences in the distribution of metal-centered electrons and that these differences are a consequence of the changes in geometry of the macrocyclic ligand. This can be straightforwardly addressed in terms of angular overlap model (AOM) considerations,[45] assuming that electron−electron repulsions dominate interactions in the d^9 complexes (paragraph S29[37]). The increases in magnetic coupling with decreases of the N−Cu−N angle, from ~180° (square pyramidal) to ~120° (trigonal bipyramidal) can be associated with increasing accessibility of an electronic configuration that directly overlaps the SOMO with the bridging ligand σ orbitals.

C. Models for Magnetic Coupling. 1. Three-Center Bonding Model.[46] In the limit of very strong bridging-ligand-mediated metal−metal coupling, it is conceptually useful to treat the magnetic properties of the different complexes in terms of a three-center, four-electron bonding contribution to the ground state. For simplicity, this can be formulated in terms of mixing an axial (with respect to the macrocyclic ligand) M orbital of each metal (Cu(a) and Cu(b)) with a bridging ligand orbital as in

$$\Psi_B = [(2)^{-1/2}(\psi_{Cu(a)} - \psi_{Cu(b)}) + \alpha_{ML}\psi_L]N \quad (5a)$$

$$\Psi_N = [\psi_{Cu(a)} + \psi_{Cu(b)}](2)^{-1/2} \quad (5b)$$

$$\Psi_A = [(2)^{-1/2}\alpha_{ML}(\psi_{Cu(a)} - \psi_{Cu(b)}) - \psi_L]N \quad (5c)$$

$$N = (1 + \alpha_{ML}{}^2)^{-1/2}$$

In these equations, $\alpha_{ML} = H_{ML}/E_{ML}$ (H_{ML} is the mixing matrix element and E_{ML} the vertical LMCT energy) and the Ψ_K corresponds to the molecular orbital bonding, nonbonding, and antibonding components (K = B, N, and A), respectively. The singly occupied metal-centered orbital is in the plane of the MCL ligand in the monometal Cu(MCL) complex, and the axial ($d\sigma_\perp$) orbital is fully occupied. The electronic configuration with a partly occupied $d\sigma_\perp$ orbital is a relatively high-energy electronic excited state of these complexes (a ligand field excited state with $h\nu_{max} \approx 20 \times 10^3$ cm^{-1}).[47] However, as the molecule folds along a N−Cu−N diagonal axis, from an approximately square planar to an approximately trigonal bipyramidal geometry, this is no longer the case. The AOM indicates that there can be a low-energy configuration with a partly occupied metal-centered orbital available in the remaining position in the trigonal plane. The AOM calculation indicates that this configuration becomes the lowest energy electronic configuration for an N′−M−N′ angle between 135° and 120°. To the extent that such an electronic configuration contributes to the ground state, the Cu^{II}−X−Cu^{II} interaction is equivalent to a three-center, four-electron bonding interaction and consistent with the observed antiferromagnetic coupling in the trigonally distorted complexes (see Figure 4). The actual "bond energy" associated with this mixing mechanism at the second-order perturbation theory level is $H_{BB} = \alpha_{ML}{}^2E_{ML} = (H_{ML})^2/E_{ML}$. For the $[\{Cu(tet\textit{b})\}_2Cl]^{3+}$ complex, we estimate (for F = Faraday's constant) that $E_{ML} \approx \{F[E_{1/2}(Cl^{\bullet}/Cl^-) - E_{1/2}(Cu^{II}/Cu^{I})] + \lambda_r\}$[48] and $\lambda_r \approx 8 \times 10^3$ cm^{-1} so that $E_{ML} \approx 32 \times 10^3$ cm^{-1}, and $J = -144$ cm^{-1} implies that $H_{ML} \approx 2 \times 10^3$ cm^{-1} (assuming $2H_{BB} = -J$ and that in this limit the two-electron magnetic coupling is proportional to

(42) Mingos, D. M. P. *Essential Trends in Inorganic Chemistry*; Oxford University Press: New York, 1998.
(43) Jungst, R.; Stuckey, G. *Inorg. Chem.* **1974**, *13*, 2404.
(44) Bauer, R. A.; Robinson, W. R.; Margerum, D. W. *J. Chem. Soc., Chem. Commun.* **1973**, 289.
(45) Lever, A. B. P.; Solomon, E. I. In *Electronic Structure and Spectroscopy of Inorganic Comounds*; Solomon, E. I., Lever, A. B. P., Eds.; Wiley: New York, 1999; Vol. I, p 1.
(46) Cotton, F. A. *Chemical Applications of Group Theory*, 3rd ed.; Wiley: New York, 1990.
(47) Lever, A. P. B. *Inorganic Electronic Spectroscopy*; Elsevier: Amsterdam, 1984.
(48) Endicott, J. F. *Electron Transfer in Chemistry*; Balzani, V., Ed.; Wiley-VCH: New York, 2001; Vol. 1, p 238.

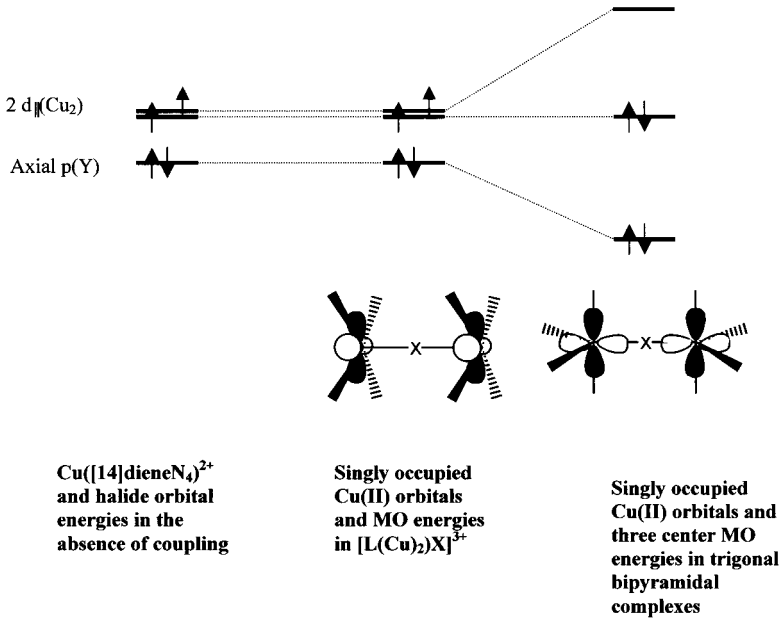

Figure 4. Qualitative representation of halide-mediated Cu(II)/Cu(II) coupling in halo-bridged square pyramidal (center) and trigonal bipyramidal (right) complexes. The ground-state singlet electronic configuration has been selected for emphasis. The ground-state singlet−triplet energy difference is relatively small (compared to k_BT; ambient conditions) for the complexes discussed in this paper.

the product of one-electron metal/ligand coupling matrix elements).[23] This corresponds to good Cu^{II}/Cl^- orbital overlap (with H_{IJ} proportional to the overlap integral S_{IJ}).[13,49,50] In contrast, these same parameters and the very weak magnetic coupling in the complexes that we report here implies that $H_{ML} < 0.3 \times 10^3$ cm^{-1}, consistent with this simple model and poor Cu^{II}/X^- orbital overlap. This poor orbital overlap is readily attributed to the near-orthogonality of the partly occupied orbitals to the bridging axis. However, we observe intense LMCT absorptions in these systems, suggesting[13,51,52] that H_{ML} is more than 15 times larger than the value inferred above. Therefore, this model does not adequately describe these systems.

Before discussing a different model, we consider a possible basis for the apparently contradictory inferences about H_{ML}.

2. Some Symmetry Considerations. For the face-to-face dimers in C_{2v} symmetry (the molecular C_2 axis is the symmetry-based *z* axis and passes through the halide parallel to the macrocycle rings), the unpaired electrons are in the planes of the macrocyclic ligand rings. The ground-state SOMOs have $d\sigma_{||}$ orbital symmetries of a_2 and b_1 in an electronically coupled system. The p orbital symmetries of the bridging halide are a_1, b_1, and b_2. Only the b_2 orbital overlaps significantly with metal orbitals (filled metal orbitals in the present systems). Thus, halide-mediated three-center mixing of the half-filled $d\sigma_{||}$ orbitals of the face-to-face Cu(II) dimers is not allowed (a weak δ interaction could result from $b_1(p_x)/b_1(d\sigma_{||})$ orbital overlap).

For a largely ionic interaction of the halide with the Cu(II) center, electron−electron repulsions along the molecular *z* axis could polarize the p-orbital electron density so that the p_x and p_y orbitals of the halide might be more realistically considered to be rotated off the molecular Cartesian axes by about 45°. The resulting orbital combination with B_1 symmetry would have some spatial overlap with the (B_1 symmetry) $d\sigma_{||}$ orbitals. The resulting angular overlap would be roughly similar to $d\pi/p\pi$ overlap, consistent with the observation that the LMCT absorptivities observed in these systems are only about twice those of the comparable $Ru(NH_3)_5X^{2+}$ complexes.[53,54]

3. Superexchange Model for Magnetic Coupling. Weihe et al.[24] and Brunold et al.[20] have recently discussed bridging-ligand-mediated, metal−metal magnetic coupling in terms of a fourth-order perturbation theory energy contribution arising from superexchange coupling. For the case that each metal contains a half-filled atomic orbital that couples to the bridging ligand, the contribution to *J* is given by the equation[20,24]

$$-2J \cong 4(H_{XL}H_{YL}/\Delta)^2(U^{-1} + \Delta^{-1}) \cong (H_{MM'}^{spx})^2/U \quad (6)$$

where the H_{KL} (K = X or Y) are the metal−ligand coupling matrix elements for the metals X and Y, Δ is the vertical LMCT energy, U is the vertical energy for metal-to-metal electron transfer (defined in terms of ionization energies[24]), and $H_{MM'}^{spx}$ is the superexchange contribution to the metal-to-metal electron-transfer coupling matrix element (the parameters are defined a little differently in the ligand-mediated coupling in electron-transfer systems).[16−18,20] In effect, eq 6 defines the two-electron magnetic coupling in terms of a product of one-electron matrix elements,[20,24] and these are the same matrix elements used to describe coupling in electron-transfer systems.[17,18,20]

D. Cu(II)/Cu(III) and Cu(I)/Cu(II) Electron-Transfer Systems. The mechanism for magnetic coupling described in the preceding section involves configurational mixing of the $[L(Cu^{II})_2X]^{3+}$ ground state with the $[L(Cu^ICu^{III})X]^{3+}$ electron-transfer excited state:

$$\{Cu^{II}(X^-)Cu^{II}\}_G + h\nu \rightarrow \{Cu^I(X^-)Cu^{III}\}_E \quad (7)$$

To pursue the issues involved, we have performed some studies of both the Cu^{III}/Cu^{II} and Cu^{II}/Cu^I electron-transfer couples.

The one electron-transfer process in eq 7 and the extent of the bridging-ligand-mediated mixing of a $\{Cu^{III}(X^-)Cu^I\}_E$ electronic configuration into the ground-state $\{Cu^{II}(X^-)Cu^{II}\}_G$

(49) Bersuker, I. B. *Electronic Structures and Properties of Transition Metal Compounds*; Wiley: New York, 1996.
(50) Zahradnik, R.; Polak, R. *Elements of Quantum Chemistry*; Plenum: New York, 1980; p 196.
(51) Hush, N. S. *Electrochim. Acta* **1968**, *13*, 1005.
(52) Hush, N. S. *Prog. Inorg. Chem.* **1968**, *8*, 391.

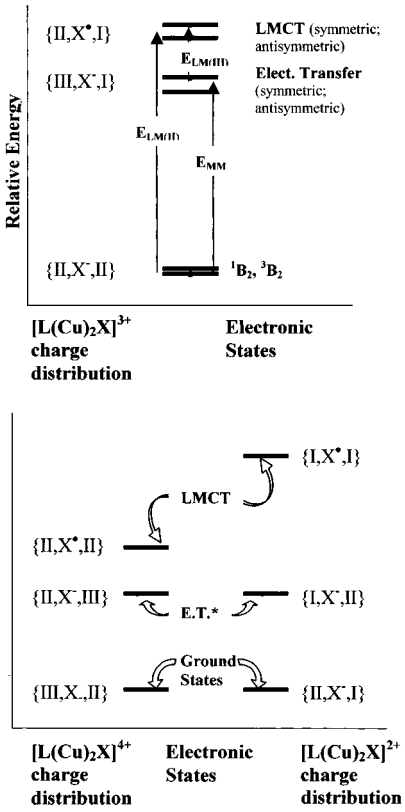

Figure 5. Energy schemes for dicopper complexes: (top) the states important for magnetic coupling in $[L(Cu^{II}Cu^{II})X]^{3+}$; (bottom) the states important in the degenerate electron-transfer coupling in $[L(Cu^{III}Cu^{II})X]^{4+}$ and $[L(Cu^{II}Cu^{I})X]^{2+}$.

wave function can be described in terms of conventional electron-transfer arguments;[14,17,55,56] these are qualitatively illustrated in Figure 5. The amount of this excited character in the ground state is expected to be proportional to $\alpha_{GE}^2 = [H_{MM}^{spx}/E_{MM}]^2$, where E_{MM} is the vertical energy difference between the metal-to-metal electron-transfer states. In these symmetric two-electron complexes, the ground state has either singlet or triplet spin multiplicity and B_1 electronic orbital symmetry. Mixing of the ground state with the $^1\{Cu^{III}Cu^{I}\}$ excited state would stabilize the $^1B_1$ state by an amount $\epsilon_s(Cu^I/Cu^{III})$ given by

$$\epsilon_s(Cu^I/Cu^{III}) = (H_{MM}^{spx})^2/E_{MM} \quad (8)$$

The superexchange matrix element is usually expressed in terms of parameters defined for the isolated pairs of components.[17,20] For this purpose we define matrix elements and vertical energies for the component couples: (1) $H_{LM(II)}$ and $E_{LM(II)}$ for $\{Cu^{II},X^-\} \rightarrow \{Cu^I,X^\bullet\}$; (2) $H_{LM(III)}$ and $E_{LM(III)}$ for $\{Cu^{III},X^-\} \rightarrow \{Cu^{II},X^\bullet\}$; and (3) H_{MM} and E_{MM} for $\{Cu^{II},Cu^{II}\} \rightarrow \{Cu^ICu^{III}\}$. The energies may then be defined in terms of half-wave potentials and reorganizational energies (λ_r(M,N); this is interpreted as a free energy quantity here) as in the following equations ($\alpha_{IJ} = H_{IJ}^{spx}/E_{IJ}$).[48,57,58]

$$E_{MM} \cong F[E_{1/2}(Cu^{III}/Cu^{II}) - E_{1/2}(Cu^{II}/Cu^{I})] + {}^1/_2[\lambda_r(Cu^{III}/Cu^{II}) + \lambda_r(Cu^{II}/Cu^{I})](1 - 2\alpha_{MM}^2) \quad (9)$$

$$E_{LM(II)} \cong F[E_{1/2}(X^\bullet/X^-) - E_{1/2}(Cu^{II}/Cu^{I})] + {}^1/_2[\lambda_r(X^\bullet/X^-) + \lambda_r(Cu^{II}/Cu^{I})](1 - 2\alpha_{LM(II)}^2) \quad (10)$$

$$E_{LM(III)} \cong F[E_{1/2}(X^\bullet/X^-) - E_{1/2}(Cu^{III}/Cu^{II})] + {}^1/_2[\lambda_r(X^\bullet/X^-) + \lambda_r(Cu^{III}/Cu^{II})](1 - 2\alpha_{LM(III)}^2) \quad (11)$$

Parameter values for the $(X^\bullet/X^-)$ couples, based in part on ion pair charge-transfer spectra, have been tabulated.[48,57] The empirical parameters for the copper couples can be obtained from direct measurement or inferred from the related ion pair spectroscopic analysis.[48] The corrections in α_{IJ} arise from a perturbation theory evaluation of the differences in species in eqs 7 and 9−11 (paragraph S30).[37,48,59] In principle, the same set of parameters can be related to the component mixed valence, $\{Cu^{II}(X^-)Cu^I\}$ and $\{Cu^{III}(X^-)Cu^{II}\}$, electron-transfer couples.

Electronic coupling in the mixed-valence complex is expected to give rise to a separation, $\Delta E_{1/2}$, of the half-wave potentials for the successive one-electron oxidations of $[L(Cu)_2X]^{3+}$. In the limit of a valence-localized system, the relationship between $\Delta E_{1/2}$ and H_{AB} can be based on the comproportionation constant, K_c (eq 12) because

$$[L(Cu^{II}Cu^{II})X]^{3+} + [L(Cu^{III}Cu^{III})X]^{5+} \overset{K_c}{\rightleftharpoons} 2[L(Cu^{II}Cu^{III})X]^{4+} \quad (12)$$

$RT \ln K_c$ is expected to increase with perturbational stabilization energy, $\epsilon_{DA} = H_{DA}^2/E_{DA}$.[13,14,60] However, other factors also contribute to K_c. Important among these are: (1) a statistical factor ($K_c \rightarrow 4$ if no other factors contribute);[14] (2) changes in the densities of vibrational states and spin multiplicity that accompany the oxidation and reduction;[61] (3) changes in electrostatic repulsion[14,60] and solvation;[62] and (4) changes in magnetic coupling.[63,64] Only the statistical factor ($g_s \approx 35$ mV) is usually considered. If the ground state of the mixed-valence system is delocalized, some variation of a three-center bonding model is more appropriate.

On the basis of $\Delta E_{1/2} \leq 30$ mV for the oxidation of $[L(Cu)_2Cl]^{2+}$, we infer that the ground state of $[L(Cu^{III}Cu^{II})Cl]^{3+}$ is localized and that $H_{DA} < 3 \times 10^2$ cm^{-1} for this complex (with $E_{DA} \cong \lambda_r(Cu^{III}/Cu^{II}) \approx 12 \times 10^3$ cm^{-1}). This assumes the same contribution to reorganizational energy from each electron added to the $d\sigma_{||}$ orbital, or $\lambda_r(Cu^{III}/Cu^{II}) \approx \lambda_r(Cu^{II}/Cu^{I})$. For a chloride-mediated superexchange pathway, with $h\nu_{max}(Cl^-/Cu^{III}\ LMCT) \cong 24 \times 10^3$ cm^{-1} (based on observed X^-/Cu^{II}(MCL) LMCT transitions and corrected for the difference in $E_{1/2}$ for the Cu^{III}/Cu^{II} and Cu^{II}/Cu^{I} couples), we estimate that $H_{LM(III)} \lesssim 3 \times 10^3$ cm^{-1}. Although the irreversibility of the electrochemical reductions of the Cu^{II}(MCL) complexes does not permit an accurate evaluation of $E_{1/2}(Cu^{II}/Cu^{I})$, there is no evidence of any stabilization by the bridging halide, and the

(53) Verdonck, E.; Vanquickenborne, L. G. *Inorg. Chem.* **1974**, *13*, 762.
(54) Hartmann, H.; Buschbeck, C. *Z. Phys. Chem. Frankfurt* **1957**, *11*, 120.
(55) Sutin, N. *Progr. Inorg. Chem.* **1983**, *30*, 441.
(56) Sutin, N. *Adv. Chem. Phys.* **1999**, *106*, 7.
(57) Gorelsky, S. I.; Kotov, V. Y.; Lever, A. B. P. *Inorg. Chem.* **1998**, *37*, 4584.
(58) Lever, A. B. P.; Dodsworth, E. In *Electronic Structure and Spectroscopy of Inorganiic Compounds*; Lever, A. B. P., Solomon, E. I., Eds.; Wiley: New York, 1999; Vol. II.
(59) Endicott, J. F.; Uddin, M. J. *Coord. Chem. Rev.*, in press.
(60) Sutton, J. E.; Taube, H. *Inorg. Chem.* **1981**, *20*, 4021.
(61) Richardson, D. E.; Sharpe, P. *Inorg. Chem.* **1993**, *32*, 1809.
(62) Watzky, M. A.; Macatangay, A. V.; Van Camp, R. A.; Mazzetto, S. E.; Song, X.; Endicott, J. F.; Buranda, T. *J. Phys. Chem.* **1997**, *101*, 8441.
(63) Evans, C. E. B.; Yap, G. P. A.; Crutchley, R. J. *Inorg. Chem.* **1998**, *37*, 6161.
(64) Endicott, J. F.; Watzky, M. A.; Song, X.; Buranda, T. *Coord. Chem. Rev.* **1997**, *159*, 295.

Table 7. Electrochemical Data of the Complexes[a]

complex	couple	scan rate (mV/s)	CV (V) E_{pc}	CV (V) E_{pa}	DPP (V)	ΔE(DPP) (V)
$[Cu([14]dieneN_4]^{2+}$	(III)/(II)	400	0.60	0.66	0.63	
$[L(Cu)_2Br]^{3+}$	(III,II)/(II,II)	25	0.84	1.00	0.93	0.26
$[L(Cu)_2Br]^{3+}$	(III,III)/(III,II)	25	1.13	1.27	1.19	
$[L(Cu)_2Br]^{3+}$	(II,II)/(I,I)	400		−0.92[b]		
$[L(Cu)_2Cl]^{3+}$	(III,II)/(II,II)	400	0.67	0.77	0.695	0.025
$[L(Cu)_2Cl]^{3+}$	(III,II)/(III,III)	400	*c*	*c*	0.72	
$[L(Cu)_2Cl]^{3+}$	(II,II)/(I,I)	400		−0.86[b]		
$[L(Cu)_2]^{4+}$	(III,III)/(II,II)	400	(∼0.4)[d]	∼0.8[e]		

[a] In acetonitrile with tetrabutylammonium hexafluorophosphate, 1 M, Pt working electrode and Ag/AgCl reference electrode. All potentials referenced are to $Fe(Cp)_2^{+,0}$, $E_{1/2} = 0.437$ V vs SCE (Bard, A. J.; Falkner, L. R. *Electrochemical Methods. Fundamentals and Applications*; Wiley: New York, 1980.). [b] Very irreversible; the only anodic waves observed were associated with CuX or Cu^0. See text. [c] Separate wave was not resolved. [d] Value depended on sweep rate and scan range. [e] Very irreversible.

Table 8. Macrocyclic Ligand Coordination and Magnetic Coupling

complex	reference	∠N(2)−Cu−N(4), deg	Cu−Cu distance, Å	Cu coordination geometry	J, cm^{-1}
$Cu_2(tet\ b)_2Cl](ClO_4)_3$	45	111	5.0	trigonal bipyramid	−144
$Cu_2([14]\text{-}4,1\text{-}dieneN_4)_2CN](ClO_4)_3$	44	134.6(1)	5.4	trigonal bipyramid	−4.8
$[Cu_2LCl](ClO_4)_3$	this work	163.9(2)	5.077	square pyramid	−0.47
$[Cu_2LBr](PF_6)_3$	this work	165.4(2)	5.340	square pyramid	−0.58

cathodic peaks for these reductions are all about the same shape and potential (about −0.9 V vs Ag/AgCl in acetonitrile).

These electron-transfer parameters can be used to evaluate H_{MM}^{spx} in eq 8 and thus to evaluate consistency with the inferences from the magnetic measurements. Standard superexchange coupling arguments[17,18] lead to

$$H_{MM}^{spx} \cong \frac{H_{LM(II)}H_{LM(III)}(E_{LM(III)} + E_{LM(II)})}{E_{LM(III)}E_{LM(II)}} \qquad (13)$$

for the halide-mediated coupling of the $\{Cu^{II},Cu^{II}\}$ and $\{Cu^{III}\text{-}Cu^{I}\}$ configurations. In the limit that $E_{LM(III)} \approx E_{LM(II)}$ (E_{MM} small), eq 13 reduces to

$$H_{ge}^{spx} \cong 2H_{LM(III)}H_{LM(II)}/E_{LM(II)} \qquad (14)$$

and eq 8 can be represented as

$$|J| \approx \frac{4(H_{LM}^{II,X}H_{LM}^{I,X}/E_{LM}^{I,X})^2}{E_{MM}} \qquad (15)$$

This is essentially the same as eq 6 for $\Delta \gg U$. This limit does not hold for the systems described here (it should be noted that we have defined vertical energy quantities in terms of eqs 9−11, as is common,[48,58,59] while Solomon and co-workers[19,20] have used a very different means of evaluating those energies). The substitution of the electron-transfer parameters obtained for the $[L(Cu)_2Cl]^{3+}$ complex into eqs 8 and 13 gives $H_{MM} = H_{MM}^{spx} < 1.3 \times 10^3$ cm^{-1} and $|J| < 8$ cm^{-1}; for $[L(Cu)_2Br]^{3+}$ we estimate $|J| \approx 2$ cm^{-1} (based on the corresponding parameters for this complex; see Table 9). This is in good agreement with the magnetic measurements.

The oxidations of $[L(Cu^{II})_2Br]^{3+}$ appear as two well-defined, quasi-reversible CV waves (or DPP peaks) with $\Delta E_{1/2} = 210$ mV. This implies appreciable Br^--mediated Cu^{III}/Cu^{II} electronic coupling; arguments similar to those presented above indicate that $H_{DA}(Cu^{II}/Cu^{III}) \cong 1.1 \times 10^3$ cm^{-1}. One interpretation of this behavior that is consistent with points made above is that the Cu(III) has a partly filled $d\sigma_\perp$ orbital in this complex. This would correspond to a high-spin d^8 Cu(III) species; this is analogous to the conversion of the low-spin d^8 Ni(II) analogue

Table 9. Estimates of Parameters Relevant to Magnetic and Electronic Coupling in the Face-to-Face Copper Dimers

parameter[a]	X = Cl^-	X = Br^-
A. Formal Charge of Ground State: (II,X^-,II)		
E_{MM}[b]	28	28
$E_{LM(II)}$	40[c]	36[d]
$E_{LM(III)}$[e]	12	8
$F\Delta E_{1/2}$[f]	16	16
$\lambda_r(Cu^{II},Cu^{II}/Cu^{I}Cu^{III})$	12	12
$H_{LM(II)}$	<3	∼2
H_{MM}[h]	<1.3	≤0.17[i]
	≤0.17[i]	
$\lvert J\rvert$[j]	<0.004	
B. Formal Charge of Ground State: (III,X^-,II)		
$E_{LM(III)}$[k]	24	20
$E_{LM(III)}$*[l]	12	8
ϵ_s[m]	<0.02	0.73
$\lambda_r(Cu^{III},Cu^{II}/Cu^{II},Cu^{III})$[g]	12	12
H_{MM}[n]	≤0.5	3
$H_{LM(III)}$[o]	<4	8
C. Formal Charge of Ground State: (II,X^-,I)		
$E_{LM(II)}$[k]	40[c]	36[d]
$E_{LM(II)}$*[l]	28	24
ϵ_s[m]	<0.3	<0.3
$\lambda_r(Cu^{II}Cu^{I},Cu^{I}Cu^{II})$[g]	12	12
H_{MM}[n]		<2
$H_{LM(II)}$		∼10 (spectra)[p]
		<3 ($F\Delta E_{1/2}$)[o]

[a] All energies in units of $cm^{-1}/10^3$. [b] Based on eq 9, measured differences in half-wave potentials of the $Cu([14]dieneN_4)^{3+,2+}$ and $Cu([14]dieneN_4)^{2+,1+}$ couples, $\alpha_{MM} \approx 0$, and reorganizational energies estimated from ion-pair CT spectra (paragraph S30[37]). [c] Based on the LMCT absorption maximum for $[L(Cu)_2Br]^{3+}$ and the difference typical of $X^- \rightarrow M$ ($p\pi/d\pi$) LMCT transitions for X = Cl and Br (ref 49 and Figure S13[37]). [d] Table 4. [e] Vertical energy for (Cu^{II},X^-,Cu^{II}) ground-state coordinates: $E_{LM(II)}^* = (E_{LM(II)} - E_{MM}) \cong \{E_{LM(II)} - F[E_{1/2}(Cu^{2+,+}) - E_{1/2}(Cu^{3+,2+})]\}$. [f] See paragraph S30.[37] [g] Based on IPCT spectra and eq 9; see paragraph S30.[37] [h] Based on eq 13. [i] Assuming that $|J| \leq 1$ cm^{-1}. [j] Based on eq 12. [k] Vertical energy for (III,X^-,II) ground-state coordinates: $E_{ML}^{II,X} = \{E_{ML}^{I,X} - F[E_{1/2}(Cu^{2+,+}) - E_{1/2}(Cu^{3+,2+})]\}$. [l] Excited-state energy difference evaluated with respect to the vibrationally equilibrated coordinates: $E_{ML}^{*32} = \{E_{ML}^{32} - \chi_r\}$. [m] Ground-state stabilization from mixing of electron-transfer states: $\epsilon_s = (1/2)RT\ln(K_c/4) = (F\Delta E_{1/2} - g_s)/2$. [n] Based on $RT\ln(K_c/4) = 2H_{DA}^2/E_{DA}$. [o] $E_{ML}^* = (E_{ML(II)} - \chi_r)$. [p] Based on refs 2−4.

(65) Udugala-Ganenenege, M. Y. Ph.D. Dissertation. Wayne State University, Detroit, MI, 2000.
(66) Udugala-Ganehenege, M. Y. Work in progress.

to high-spin upon association with halides.[65] The issues raised by this behavior will be discussed in more detail in our report on the $[L(Ni)_2X]^{n+}$ complexes.[66]

D. Summary and Conclusions

The face-to-face $[L(Cu([14]dieneN_4))_2X]^{n+}$ complexes have allowed us to investigate some issues of the dependence of metal-to-metal electronic coupling on the spatial distribution of the donor and acceptor orbitals. This work has confirmed that electronic coupling tends to be weak if the donor and acceptor orbitals are approximately orthogonal to the metal−(bridging ligand)−metal axis, even in complexes with a single halide bridge. The comparison with previous (kinetic or magnetic) studies of closely related halide (or cyanide) bridged dicopper complexes suggests that the coupling is enhanced by molecular geometries that place donor and/or acceptor orbitals along the bridging axis.

The largest values of $H_{LM(II)}$ consistent with the magnetic or electrochemical measurements on $[L(Cu)_2Cl]^{3+}$ and a three-center bonding (or second-order perturbation theory) model would imply an absorptivity of the LMCT band of this complex that is about 5% of the observed intensity. This contrast results from a difference between the mixing matrix elements appropriate to the spectroscopic measurements and those appropriate to the magnetic and electrochemical measurements. The H_{LM} parameters implicit in the superexchange description of the metal−metal coupling in these complexes agree reasonably well with the spectroscopic results. Thus, the $[L(Cu)_2X]^{3+}$ complexes nicely illustrate the contrasts between different halide-mediated mixing mechanisms, and they also illustrate the relationship and contrasts between metal/ligand coupling and ligand-mediated metal/metal coupling. We are not aware of previous studies of the bridging mediated coupling of two metals that has so simply demonstrated the contrasts among simple two-center mixing, three-center mixing, and superexchange mixing and the way in which each of these mechanisms depend on local metal/ligand mixing.

Acknowledgment. The authors thank the Office of Basic Energy Sciences of the Department of Energy for partial support of this research. We gratefully acknowledge Professor Ratna Naik of the Department of Physics for making the ESR measurements.

Supporting Information Available: Tables of crystal data, atomic parameters, bond lengths and angles, anisotropic displacement parameters, and hydrogen coordinates for compounds **1** and **2** in CIF format; mass spectra for complexes **1** and **2**; visible−UV spectroscopic changes accompanying ion association with $[L(Cu)_2]^{4+}$; absorbance changes accompanying the formation of $[L(Cu)_2Br]^{3+}$; method for determining ion-pair association constant; absorption spectra of the complexes; IR spectrum of **1**; cyclic voltammograms for **1**−**3**; inverse magnetic susceptibility and effective magnetic moment as a function of temperature; AOM analysis; perturbation theory analysis. This material is available free of charge via the Internet at http://pubs.acs.org.

IC000726W